

# Geosynchronous Debris Conjunction Lead-Time Requirements for Autonomous Low-Thrust Disposal Guidance

Paul V. Anderson<sup>1</sup> · Hanspeter Schaub<sup>1</sup>

© American Astronautical Society 2016

**Abstract** Autonomous, low-thrust guidance for active disposal of geosynchronous debris, subject to collision avoidance with the local debris population, is studied. A bisection method is employed to determine trajectory modifications to avoid a conjunction debris object by a range of distances, assuming a range of collision lead times. A parametric study is performed, in which re-orbit thrust accelerations are varied from  $10^{-6}$  to  $10^{-3}$  m/s<sup>2</sup>, to demonstrate how the continuous-thrust level impacts the required lead time to achieve a desired debris miss distance. The lowest thrust levels considered show that a 6-12 hour lead time is required to achieve a 1-10 km debris separation at the predicted collision time.

**Keywords** GEO space debris · Collision avoidance · Low-thrust maneuvers

## Introduction

The geostationary (GEO) regime is a unique commodity of the terrestrial satellite industry that is becoming increasingly contaminated with orbital debris, [1, 2] but is heavily populated with high-value assets.[3] As the lack of atmospheric drag effects at the GEO altitude renders lifetimes of these debris essentially infinitely long, conjunction assessment must be performed to safeguard operational GEO satellites from

---

✉ Hanspeter Schaub  
hanspeter.schaub@colorado.edu

<sup>1</sup> Department of Aerospace Engineering Sciences, University of Colorado Boulder, 429 UCB, Boulder, CO 80309, USA

potential collisions with the uncontrolled derelict population. GEO satellites must maintain a specified longitude slot, and cannot simply shift in phase to evade debris. Therefore, as the resident space object population at GEO continues to increase, the fuel cost required to remain at a particular longitude slot while performing collision avoidance with uncontrolled objects will begin to increase in tandem. Ultimately, global adherence to end-of-life mitigation guidelines must be combined with environmental remediation—active debris removal (ADR)—to curtail debris growth in this regime. Anderson and Schaub [4] The necessity for cost-effective ADR implementation in the GEO ring is becoming more prominent, especially for larger derelict objects (e.g., spent rocket bodies and non-operational payloads) that pose moderate collision risk but are a potential source of future debris growth through collisional interaction.

Proposed ADR techniques for the GEO arena typically involve re-orbiting of large-scale derelicts to “graveyard” disposal orbits at perigee altitudes above the GEO ring, factoring the GEO protection zone [5] and area-to-mass ratio of the object into the minimum altitude calculation. Jehn et al. [2], Jehn and Hernandez [6], NASA [7] A chief space-tug concept is often envisioned for performing the re-orbiting maneuver once contact with the target debris object has been established. However, as rendezvous, proximity operations, and docking with an uncontrolled—and potentially tumbling—object are challenging, several proposed methods have focused on contactless technologies such as an electrostatic tractor [8] or ion beam shepherd [9] for ADR at GEO. Each of these contactless ADR technologies call for low-thrust engines for performing the required re-orbit maneuver – the electrostatic tractor concept requires an inertial thrust proportional to the electrostatic force that is actuated on the order of mN [8], and the thrust of the ion beam shepherd concept is bounded by the performance of ion thrusters, which typically generate less than 200 mN. Bombardelli and Pelaez [9] With lower maneuverability, collision avoidance for such low-thrust re-orbit systems is challenging.

In Reference [10], the conjunction challenges for a GEO re-orbit system using low-thrust propulsion to perform orbit raising at end-of-life are investigated by quantifying the number of conjunction events possible with the current TLE population during a typical re-orbit to 300 km above GEO. In this study, it is shown that although the average number of conjunctions per trajectory rises hyperbolically as the thrust acceleration decreases, the global conjunction challenge can be reduced by (a) increasing the thrust acceleration, and/or (b) timing the start of the maneuver such that the re-orbit system begins partially or fully unsynchronized with the north-south, latitudinal motion of the local debris population. Depending on mission constraints, satellite bus design, and the particular low-thrust propulsion system used, option (a) may not be possible. Option (b) guarantees that the potential conjunction events for a given re-orbit trajectory will be reduced, but not necessarily eliminated. Therefore, it is of critical importance that such re-orbit systems be equipped with a GNC subsystem specifically for steering the vehicle onto an avoidance trajectory in the event a predicted conjunction warrants timely, evasive action. In this way, any remaining collision risk not mitigated under options (a) or (b) can be further reduced.

Although such a GNC subsystem is also beneficial for operating GEO satellites engaged in mitigation activities at end-of-life, the application to autonomous,

space-tug concepts for environment remediation is emphasized in this paper. Conceptualized in Fig. 1, an autonomous re-orbit system for ADR at GEO would approach a high-risk target derelict, dock with it via either physical or contactless means, perform a continuous-thrust burn to increase the perigee altitude per the IADC guidelines, and lastly return to the GEO altitude to repeat with other debris objects until fuel has been depleted. With lower maneuverability, however, collision avoidance for such a low-thrust re-orbit system during orbit raising is a challenging task. Conjunctions must be detected with enough lead time to sufficiently alter the trajectory of the re-orbit system to mitigate collision risk by maintaining a desired miss distance, given covariance information and a specified “no-fly” (or keep-out) zone surrounding the derelict. Intuitively, re-orbit systems with higher thrust levels (more maneuverability) can detect a conjuncting object later than systems with lower thrust levels (less maneuverability), and still miss this object by the same distance at the collision epoch. Thus, in addition to a guidance strategy for active avoidance of conjuncting debris, the re-orbit system must be equipped with the capability to sense the surrounding environment, and forecast potential conjunction events using relative state estimation and orbit prediction.

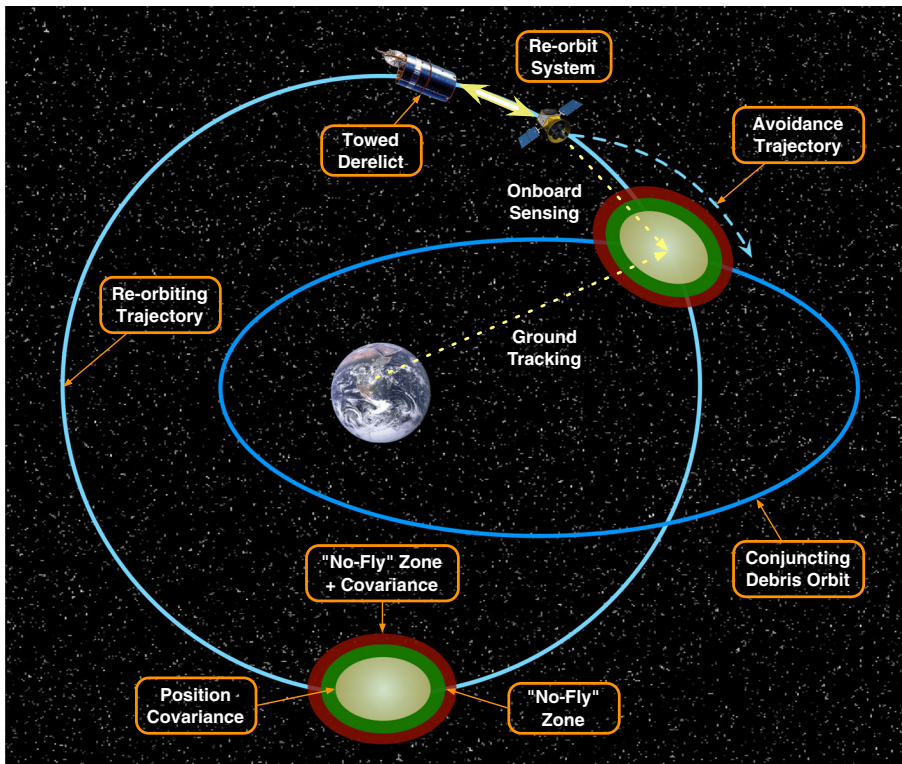


**Fig. 1** Challenges of low-thrust GEO debris re-orbit

Concepts for autonomous “sense and avoid” are widespread within the robotics and unmanned aerial vehicle communities, and have recently been applied to the challenges of spaceflight, in particular, satellite cluster flight and rendezvous and docking. The artificial potential function concept for autonomous guidance was originally developed for terrestrial robotics applications, [11, 12] and was later applied to the spacecraft formation flying problem for optimal reconfiguration, [13] distributed motion planning, [14] pattern transition, [15] and autonomous operations. Tatsch [16] In this method, an artificial potential field (that is, non-physical and for purposes of control only) is superimposed around a neighboring object, and this potential field is activated to either attract or repel the controlled vehicle to or from this object. Leonard and Fiorelli [12] Alternatively, the problem of continuous-thrust, on-orbit rendezvous can be treated by minimizing a path-dependent cost function—subject to path constraints enforcing collision avoidance among multiple vehicles—using nonlinear optimization [17, 18] or mixed-integer linear programming. Richards et al. [19] All of these intensive path-planning strategies, however, are not well-suited for autonomous GEO re-orbit systems, which demand simple-yet-robust control laws that are effective for on-orbit collision avoidance, while minimizing human-in-the-loop interactions and computational load required for the avoidance.

The guidance strategy for debris avoidance developed and simulated in this paper is analogous to the conflict resolution maneuver derived in Reference [20] for approaching aircraft in a congested control volume. It is shown that an aircraft entering the volume can always execute a lateral displacement maneuver—using a single heading change decision—that results in a conflict-free (collision-free) trajectory, as long as the width of the maneuver corridor is sufficiently large. Mao et al. [20] The guidance strategy for collision avoidance presented in this paper uses a comparable heading change, i.e., the angle of the thrust vector, to result in a conflict-free trajectory inasmuch as the lead time with which the conjuncting object is detected is sufficiently large for the maneuverability of the re-orbit system.

This paper is structured as follows. The autonomous guidance strategy for active debris avoidance during GEO re-orbit is formulated by first deriving the nonlinear equations of motion for a conjuncting debris object relative to a thrusting re-orbit system, under the assumption of two-body motion. Then, the re-orbit efficiency factor is introduced and implemented in the framework of the guidance strategy. Finally, prototype collision scenarios are generated using data from Reference [10], and the lead time requirements for the guidance strategy are evaluated in each of these representative cases.

## **Development of Guidance Strategy for Debris Avoidance**

### **Nonlinear Relative Equations of Motion with In-Plane Chief Thrusting**

Prior to formulating the guidance strategy for debris avoidance, equations of motion that describe the trajectory of a deputy debris object relative to the chief re-orbit

system—which is thrusting in the plane of the local orbit frame—are now derived.<sup>1</sup> A Cartesian coordinate parameterization of relative motion expressed in the rotating Hill frame centered on the re-orbit system is selected, since this provides a natural framework with which to formulate the guidance strategy in the context of an autonomous system using onboard sensors to scan the surrounding debris environment and onboard software to rapidly generate relative state estimates and forecast potential conjunction events. In Hill frame Cartesian coordinates, the inertial position vector of the deputy object is written as

$$\mathbf{r}_d = \mathbf{r}_c + \boldsymbol{\rho} = (r_c + x)\hat{\boldsymbol{o}}_r + y\hat{\boldsymbol{o}}_\theta + z\hat{\boldsymbol{o}}_h \tag{1}$$

where  $r_c$  is the orbital radius of the chief, and  $(x, y, z)$  are the Cartesian coordinates of the deputy object along the radial ( $\hat{\boldsymbol{o}}_r$ ), in-track ( $\hat{\boldsymbol{o}}_\theta$ ), and cross-track ( $\hat{\boldsymbol{o}}_h$ ) axes of the Hill frame. The angular velocity vector of the Hill frame  $\mathcal{O}$  relative to the inertial frame  $\mathcal{N}$  is given by

$$\boldsymbol{\omega}_{\mathcal{O}/\mathcal{N}} = \dot{f}\hat{\boldsymbol{o}}_h \tag{2}$$

where  $\dot{f} = h/r^2$  is the rate of true anomaly. Note that in-plane thrusting does not affect the angular velocity of the orbit frame  $\mathcal{O}$  directly – rather, as will be shown, in-plane thrusting in the in-track direction affects the true anomaly acceleration, which in turn affects the true anomaly rate (acceleration does not instantaneously alter velocity). Applying the transport theorem to take two derivatives of  $\mathbf{r}_d$  with respect to inertial frame: [21]

$$\begin{aligned} \ddot{\mathbf{r}}_d = & [\ddot{r}_c + \ddot{x} - \ddot{f}y - 2\dot{f}\dot{y} - \dot{f}^2(r_c + x)]\hat{\boldsymbol{o}}_r \\ & + [\ddot{y} + 2\dot{f}(\dot{r}_c + \dot{x}) + \dot{f}(r_c + x) - \dot{f}^2y]\hat{\boldsymbol{o}}_\theta + \ddot{z}\hat{\boldsymbol{o}}_h \end{aligned} \tag{3}$$

This kinematic expression can be simplified by developing expressions for the true anomaly acceleration  $\ddot{f}$  and chief radial acceleration  $\ddot{r}_c$ . Recalling that the chief angular momentum magnitude is given by  $h = r_c^2\dot{f}$ , differentiate and apply Euler’s equation  $\dot{h} = r_c a_\theta$  to show that the true anomaly acceleration is

$$\ddot{f} = -\frac{2\dot{r}_c\dot{f}}{r_c} + \frac{a_\theta}{r_c} \tag{4}$$

where  $a_\theta$  is the in-track component of the chief thrust vector  $\mathbf{a}_t = a_r\hat{\boldsymbol{o}}_r + a_\theta\hat{\boldsymbol{o}}_\theta$ . Writing the chief position in the orbit frame as  $\mathbf{r}_c = r_c\hat{\boldsymbol{o}}_r$ , and applying the transport theorem twice:

$$\ddot{\mathbf{r}}_c = (\ddot{r}_c - r_c\dot{f}^2)\hat{\boldsymbol{o}}_r + a_\theta\hat{\boldsymbol{o}}_\theta \tag{5}$$

Assuming two-body dynamics, the inertial acceleration vector of the chief is written as:

$$\ddot{\mathbf{r}}_c = -\frac{\mu}{r_c^3}\mathbf{r}_c + \mathbf{a}_t = \left(a_r - \frac{\mu}{r_c^2}\right)\hat{\boldsymbol{o}}_r + a_\theta\hat{\boldsymbol{o}}_\theta \tag{6}$$

Equating the radial components of Eqs. 5–6, the chief radial acceleration is:

$$\ddot{r}_c = r_c\dot{f}^2 - \frac{\mu}{r_c^2} + a_r \tag{7}$$

<sup>1</sup>In spacecraft formation flying nomenclature, the “chief” is the primary satellite about which all other “deputy” satellite motions are referenced.

Substituting Eqs. 4 and 7 into Eq. 3, the inertial acceleration vector of the deputy becomes:

$$\begin{aligned} \ddot{\mathbf{r}}_d = & \left[ \ddot{x} - 2\dot{f} \left( \dot{y} - y \frac{\dot{r}_c}{r_c} \right) - \dot{f}^2 x - \frac{\mu}{r_c^2} + a_r - \frac{y}{r_c} a_\theta \right] \hat{\mathbf{o}}_r \\ & + \left[ \ddot{y} + 2\dot{f} \left( \dot{x} - x \frac{\dot{r}_c}{r_c} \right) - \dot{f}^2 y + (r_c + x) \frac{a_\theta}{r_c} \right] \hat{\mathbf{o}}_\theta + \ddot{z} \hat{\mathbf{o}}_h \end{aligned} \tag{8}$$

The unforced, two-body deputy equations of motion are given by

$$\ddot{\mathbf{r}}_d = -\frac{\mu}{r_d^3} \mathbf{r}_d = -\frac{\mu}{r_d^3} (r_c + x) \hat{\mathbf{o}}_r - \frac{\mu}{r_d^3} y \hat{\mathbf{o}}_\theta - \frac{\mu}{r_d^3} z \hat{\mathbf{o}}_h \tag{9}$$

where the deputy radius is  $r_d = \sqrt{(r_c + x)^2 + y^2 + z^2}$ . Finally, equating the kinematics in Eq. 8 with the dynamics in Eq. 9 gives the exact nonlinear relative equations of motion of the deputy with respect to the chief, which admits in-plane thrusting:

$$\ddot{x} - 2\dot{f} \left( \dot{y} - y \frac{\dot{r}_c}{r_c} \right) - \dot{f}^2 x - \frac{\mu}{r_c^2} + a_r - \frac{y}{r_c} a_\theta = -\frac{\mu}{r_d^3} (r_c + x) \tag{10a}$$

$$\ddot{y} + 2\dot{f} \left( \dot{x} - x \frac{\dot{r}_c}{r_c} \right) - \dot{f}^2 y + (r_c + x) \frac{a_\theta}{r_c} = -\frac{\mu}{r_d^3} y \tag{10b}$$

$$\ddot{z} = -\frac{\mu}{r_d^3} \tag{10c}$$

Note that if thrusting is turned-off, i.e.,  $\mathbf{a}_t = \mathbf{0}$ , the relative motion equations reduce to the unforced form derived in Reference [21]. Since linearization is not applied, Eq. 10 are valid for arbitrarily large relative motion. Furthermore, Eq. 10 allow the chief orbit to be eccentric – the only assumption made in the derivation of these equations is that two-body dynamics apply for both the deputy debris object and chief re-orbit system, and the only perturbation to the chief’s orbital motion is that of the in-plane thrust vector  $\mathbf{a}_t$ .

### Efficiency Factor for Re-orbit Maneuvers

According to the Gaussian variational equations, thrusting along the instantaneous velocity vector direction generates maximum increase in the semimajor axis. Schaub and Junkins [21], Prussing and Conway [22] For the near-circular, low-thrust re-orbit trajectories considered in this study, the in-track direction is approximately oriented along the instantaneous velocity direction (i.e., small flight path angle). Assuming that the maximum available thrust acceleration  $a_{\max}$  is continuously applied during orbit raising, an *efficiency factor*  $\gamma$  for the maneuver may be defined such that the thrust vector becomes:

$$\mathbf{a}_t = a_{\max} \sqrt{1 - \gamma^2} \hat{\mathbf{o}}_r + \gamma a_{\max} \hat{\mathbf{o}}_\theta \tag{11}$$

In this formulation,  $\gamma = 1$  yields  $\mathbf{a}_t = a_{\max} \hat{\mathbf{o}}_\theta$ , that is, maximum available thrust is directed along the in-track direction for maximum increase in SMA. Applying maximum available thrust in the in-track direction is appropriate for general re-orbit maneuvers at GEO, since this minimizes the duration of the transfer, which is on the order of months for mN levels of thrust. Conversely,  $\gamma = 0$  yields  $\mathbf{a}_t = a_{\max} \hat{\mathbf{o}}_r$ , i.e.,

maximum available thrust is directed along the radial direction. Although this thrust direction still provides an increase in SMA, this rate of increase is minimal, since the Gaussian variational equation for the SMA is [21]

$$\frac{da}{dt} = \frac{2a^2}{h} \left[ e \sin(f) a_r + \frac{p}{r} a_\theta \right] \tag{12}$$

which shows that the effectiveness of the radial thrust component is reduced first by  $\sin(f)$ , then by the near-zero eccentricity (or, any thrust component not directed along the velocity vector direction does no work on the re-orbit system to increase its two-body orbit energy).

Letting  $\alpha$  be the angle in the orbit plane directed from the local radial direction  $\hat{\boldsymbol{a}}_r$ , the thrust vector of the re-orbit system can also be expressed in the form:

$$\boldsymbol{a}_t = a_{\max} \cos(\alpha) \hat{\boldsymbol{a}}_r + a_{\max} \sin(\alpha) \hat{\boldsymbol{a}}_\theta \tag{13}$$

Equating the components of Eqs. 11 and 13, the efficiency factor is  $\gamma = \sin(\alpha)$ , and is thus dependent on the angle  $\alpha$  of the thrust vector in the orbit plane. In this paper,  $\alpha$  is restricted to  $0^\circ \leq \alpha \leq 180^\circ$ , such that the thrust vector  $\boldsymbol{a}_t$  never has a component in the  $-\hat{\boldsymbol{a}}_\theta$  direction, which would serve to decrease the SMA during re-orbit via Eq. 12. Again, the goal for the autonomous guidance strategy considered in this paper is to increase the SMA to a super-synchronous disposal orbit as fast as possible, while mitigating risk incurred by conjuncting debris objects during the low-thrust transfer.

### Formulation of Bisection Guidance Strategy

In the event of a conjunction event during re-orbit that warrants timely, evasive action, a simple-yet-robust guidance strategy must be applied to autonomously alter the direction of the thrust vector to mitigate a collision. Assuming that the conjunction is detected by the re-orbit system a known time period in advance (the lead time), small modifications to the continuous-thrust trajectory of the re-orbit system can be made by the guidance subsystem early on, such that at the time of the predicted collision, the re-orbit system misses the conjuncting debris by a specified minimum distance. Therefore, the guidance strategy is formulated to tune the efficiency factor  $\gamma$ —by adjusting the in-plane angle of the thrust vector—such that the re-orbit system misses the conjuncting object by a specified distance at the predicted collision epoch, as conceptualized in Fig. 2. Note that the specified distance can be a conservative value selected *a priori*, or derived from the hard-body radii and estimated position uncertainties of the re-orbit system and conjuncting object at the time of closest approach, given a conservative probability of collision. During nominal orbit raising, the re-orbit system maintains full in-track thrusting ( $\gamma = 1$ ), but if a potential collision is forecasted at a future time, the guidance system must decrease the efficiency factor by applying a larger thrust component in the radial direction. In this manner, the rate of increase in SMA is temporarily slowed, such that the conjuncting object misses by a specified in-track distance  $y \neq 0$  when  $x = z = 0$  (the condition  $x = y = z = 0$  indicates a collision in that the deputy is at the location of the chief, i.e., the origin of the Hill frame).

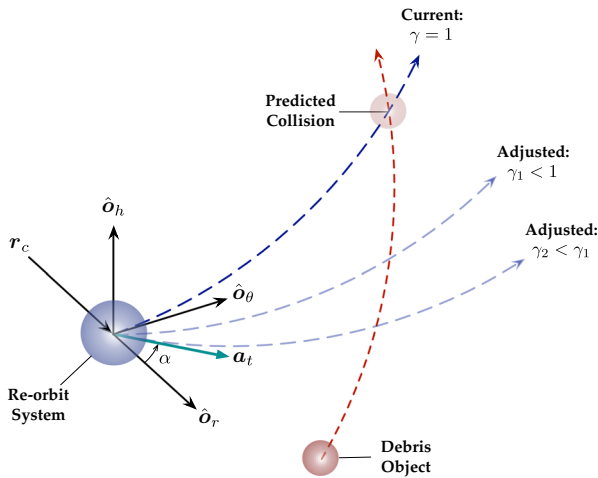


**Fig. 2** In-plane guidance concept for low-thrust debris avoidance

Inasmuch as sufficient lead time is available prior to the collision epoch given the maneuverability of the re-orbit system, a predictor-corrector method that uses (10) in tandem with a bisection root-finding method can be applied to achieve the desired miss distance. In this guidance strategy, the relative equations of motion in Eq. 10 are propagated forward to the collision epoch using the current thrust direction. The in-plane thrust angle  $\alpha$  is then iteratively adjusted via root bisection to converge on the angle  $\alpha^*$  that achieves the desired miss distance at the collision epoch. This “single-shooting” method is fast, robust, and well-suited to an autonomous re-orbiting system that uses environmental sensing to detect the debris environment prior to a potential conjunction event. A flowchart outlining the bisection guidance strategy for active debris avoidance is provided in Fig. 3. Although the algorithm as presented considers the case of a single conjuncting object only, this method can be extended to account

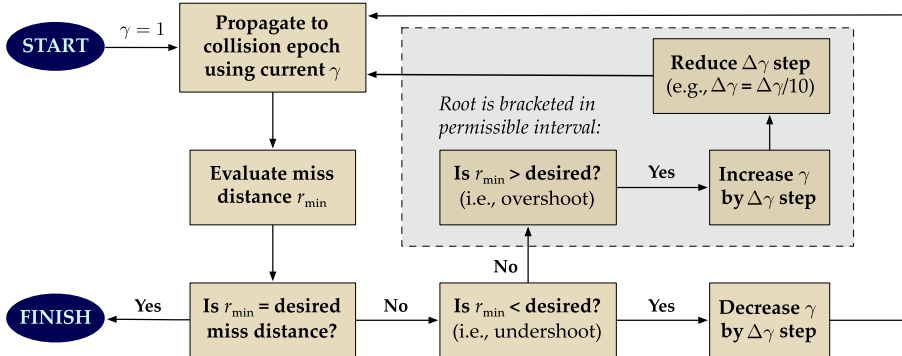


**Fig. 3** Flowchart for computer implementation of bisection guidance strategy

for multiple conjuncting objects, e.g., by maximizing the minimum miss distance over all objects at their respective times of closest approach to the re-orbit system.

Since numerical integration of Eq. 10 requires initial conditions for the conjuncting debris object, the guidance system must have knowledge of the relative trajectory of the conjuncting object in the Hill frame, which can be obtained with (a) traditional, on-ground sensing and inertial orbit determination, or (b) onboard sensing and relative orbit determination using a batch least-squares or sequential state filter, in tandem with relative range and angles measurements. Furthermore, Eq. 10 contain the chief radius  $r_c$  and radial rate  $\dot{r}_c = \dot{r}_c \cdot \hat{o}_r$ , such that the re-orbiting system must have knowledge of its own inertial position and velocity vectors, in addition to the thrust vector  $\mathbf{a}_T$  and in-plane thrust angle  $\alpha$ . This state knowledge can be obtained with (a) traditional, on-ground sensing and inertial orbit determination, (b) by applying a parametric form of position and velocity as a function of elapsed time, using the analytic results in Reference [10], for example, or (c) a combination thereof. Although not simulated in this study, the in-plane thrust angle must be updated at a predetermined frequency during the entirety of the debris approach, to account for navigation and force model errors, thruster performance uncertainties, and other error sources not modeled in the two-body framework of Eq. 10. In this manner, the *open-loop*, “single-shooting” guidance strategy becomes *closed-loop* and robust in that the desired miss distance can be achieved even in the presence of error sources and unmodeled disturbances.

Figure 4 shows several example approach geometries in the Hill frame to illustrate the effectiveness of the bisection guidance strategy for evading a conjuncting debris

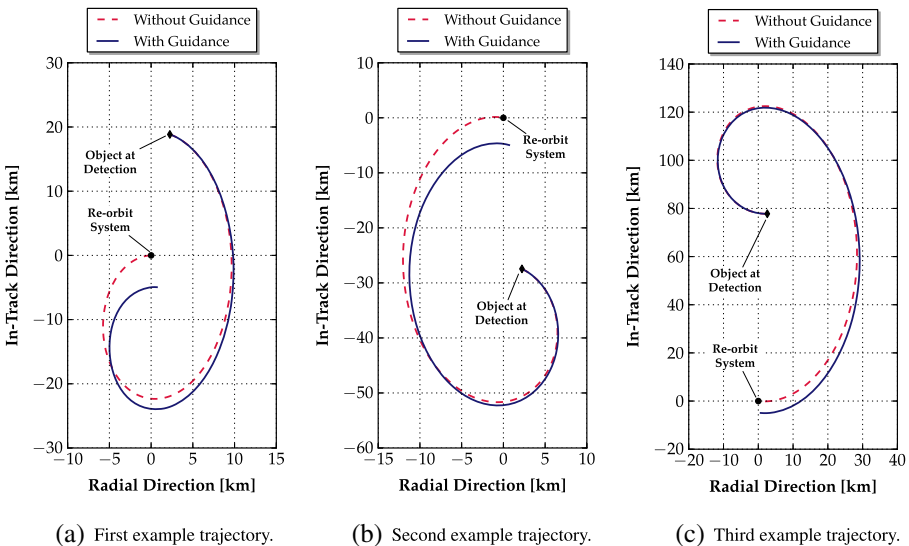


**Fig. 4** Three examples of bisection guidance, which converges on  $\gamma = 0.706$  to achieve a desired miss distance of 5 km at the predicted collision time of 24 hours out

object with low thrust propulsion. Using a 1 mN thrust level with a desired miss distance of 5 km at the simulated collision time of 24 hours from the start epoch, Fig. 4 provides propagated trajectories without guidance (i.e., in-track thrusting only), and with bisection guidance applied. In all three cases, the bisection method converges on  $\gamma = 0.706$  to achieve the specified miss distance of 5 km at the predicted collision epoch. Without the guidance law applied, a collision occurs at the origin of the Hill frame, but with bisection guidance activated, the relative trajectory of the conjuncting object is altered such that it achieves zero radial position with nonzero in-track position at the collision epoch (i.e.,  $x = 0$  with  $y \neq 0$ ).

To illustrate the effect of delaying the start time of the avoidance maneuver, Fig. 5 provides the trajectory example of Fig. 4b, if the conjuncting object is detected not 24 hours in advance of the predicted collision, but 18, 12, and 6 hours prior to the collision. In Fig. 4b, the bisection method converges on  $\gamma = 0.706$  to achieve the miss distance of 5 km. If, as in Fig. 5a, the object is detected 18 hours prior to the collision instead of 24 hours, an efficiency of  $\gamma = 0.471$  is required to maintain this 5 km separation at the collision epoch. In Fig. 5b and c, this guidance strategy does not have enough lead time to alter the relative trajectory such that 5 km separation is achieved, i.e., bisection fails because the root  $\alpha^*$  cannot be bracketed in the allowable range  $0 \leq \alpha \leq 180^\circ$ . Applying maximum available thrust in the negative radial direction ( $\gamma = 0$ ) yields a miss distance of 2.92 km for the 12-hour detection in Fig. 5b, and  $\sim 430$  m for the 6-hour detection in Fig. 5c. It is thus of critical importance to evaluate the tradeoffs among thrust acceleration, desired miss distance, and required detection time, assuming perfect knowledge in the absence of representative error sources, to establish best-case performance limits for this method.

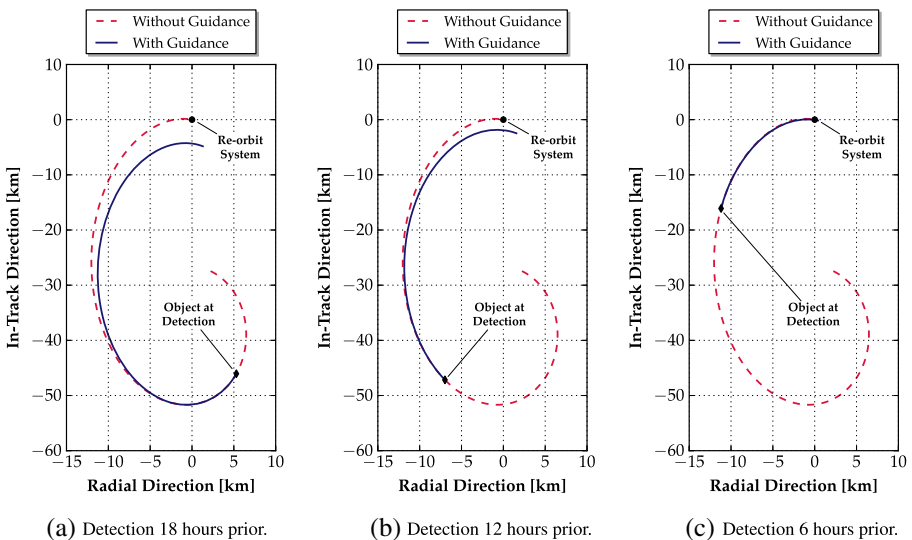


**Fig. 5** Convergence of and the efficiency factor resulting from bisection guidance are dependent on the lead time with which the object is detected prior to the collision time

## Performance of Guidance Strategy for Debris Avoidance

### Development of Prototype Collision Scenarios

To quantify best-case performance bounds for the bisection guidance method, representative approach geometries in the local Hill frame (that is, prototype conjunction geometries that a re-orbit system could encounter during orbit raising) must first be constructed. Then, these baseline scenarios are applied with a two-dimensional sweep over thrust level and miss distance, to assess the minimum detection times required to maintain the desired miss distances at the collision epoch for each surveyed thrust acceleration. Assuming two-body dynamics, Fig. 6 provides three collision scenarios that could occur for a re-orbit system during orbit raising from the GEO altitude to a super-synchronous disposal orbit:

1. *Case 1.* Collision due to a semimajor axis difference, in which the re-orbit system asymptotically approaches the object at the collision point with nearly zero relative velocity at impact (i.e., re-orbit trajectory “spirals-up” to the conjunction altitude).
2. *Case 2.* Collision due to an eccentricity difference, in which the system approaches the object at a point of intersection between two, coplanar orbits with  $e_1 \neq e_2$ , with 10's of m/s of relative velocity at impact (assuming typical eccentricities at GEO).
3. *Case 3.* Collision due to an inclination difference, in which the system approaches the object at one of the orbital nodes, i.e., points of intersection between two, non-coplanar orbits with  $i_1 \neq i_2$ , with 100's - 1000's of m/s of relative velocity at impact.

Cases 1 and 2 involve in-plane relative motion only, while Case 3 has out-of-plane relative motion. Noting that relative velocity at impact increases by an order of magnitude between each of these cases, the prototype scenarios in Fig. 6 serve as the means for comparing bisection performance bounds under successively-increasing collision velocity. Using data from the GEO re-orbit conjunctions analysis in Reference [10], Fig. 7 provides a histogram of the relative velocity for all conjunction events within 50 km detected across all seven thrust accelerations surveyed. This histogram shows an extensive range of conjunction velocities are possible for simulated continuous-thrust re-orbit trajectories. In particular, of the 4099 conjunction events detected within 50 km across all surveyed thrust levels, 80.2 % are at or above the “catastrophic” relative velocity threshold of 0.2828 km/s.<sup>2</sup> Although the simulated conjunctions in Reference [10] cannot be categorized exclusively under one of the prototype cases in Fig. 6—since conjunctions due to a combination of orbit element differences occur in practice—the histogram in Fig. 7 shows that the majority of simulated conjunctions fall under Cases 2-3 in terms of relative velocity at conjunction.

<sup>2</sup>See Reference [10] for further discussion and explicit derivation of this relative velocity threshold.

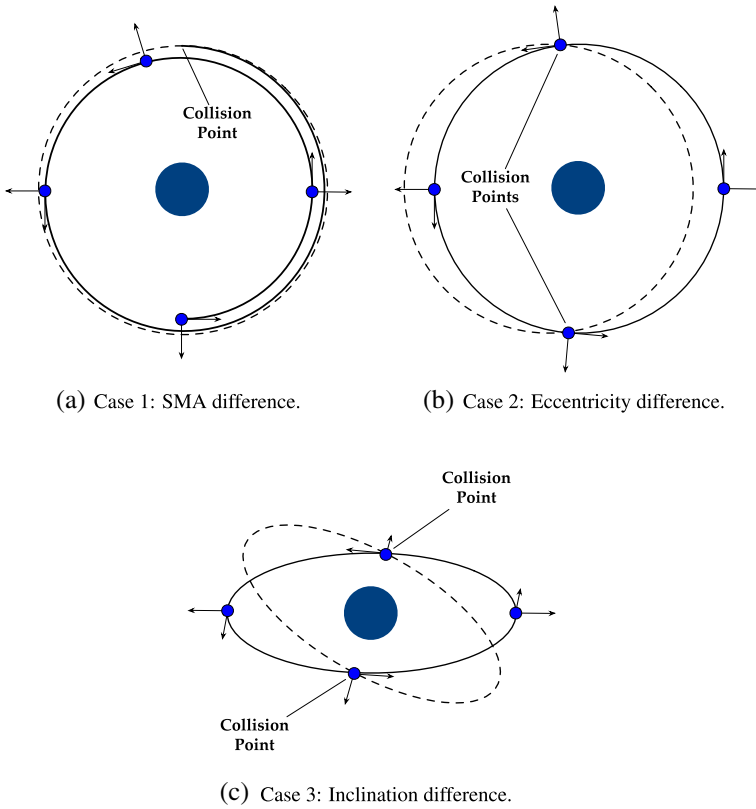


**Fig. 6** Representative GEO collision geometries for testing bisection debris avoidance strategy, where the collision speed increases from SMA case to inclination case

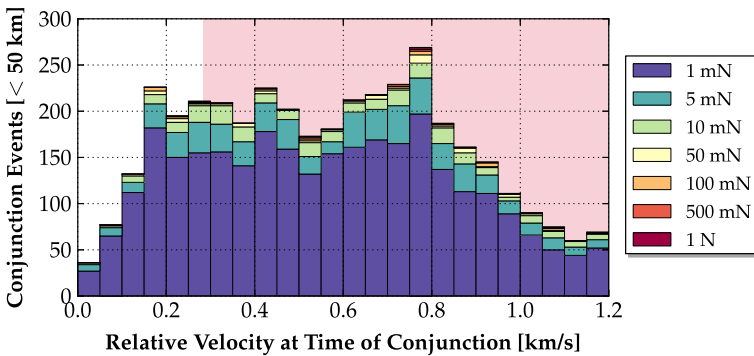


**Fig. 7** Distribution of 50 km conjunction speeds, derived from re-orbit conjunction data in Reference [10], by thrust level. Shaded region is catastrophic collision regime

To derive specific eccentricity and inclination differences to apply to these prototype collision scenarios, conjunction events from Reference [10] occurring within 10 km of the re-orbit system at the 1 mN thrust level are examined. Of the conjunction events detected at this 10 km distance threshold and thrust level, one conjunction results from an eccentricity difference  $\Delta e = 0.028$  (relative speed of 86 m/s), and another results from an inclination difference of  $\Delta i = 12.1^\circ$  (relative speed of 649 m/s). The semimajor axis difference scenario is simulated by propagating the re-orbit system forward from the GEO radius under continuous, in-track thrust until the specified collision epoch; the Cartesian state of the re-orbit system is then assigned to the conjuncting object, which is then reverse-propagated to the simulation start epoch under two-body dynamics to provide the required initial conditions. Figure 8

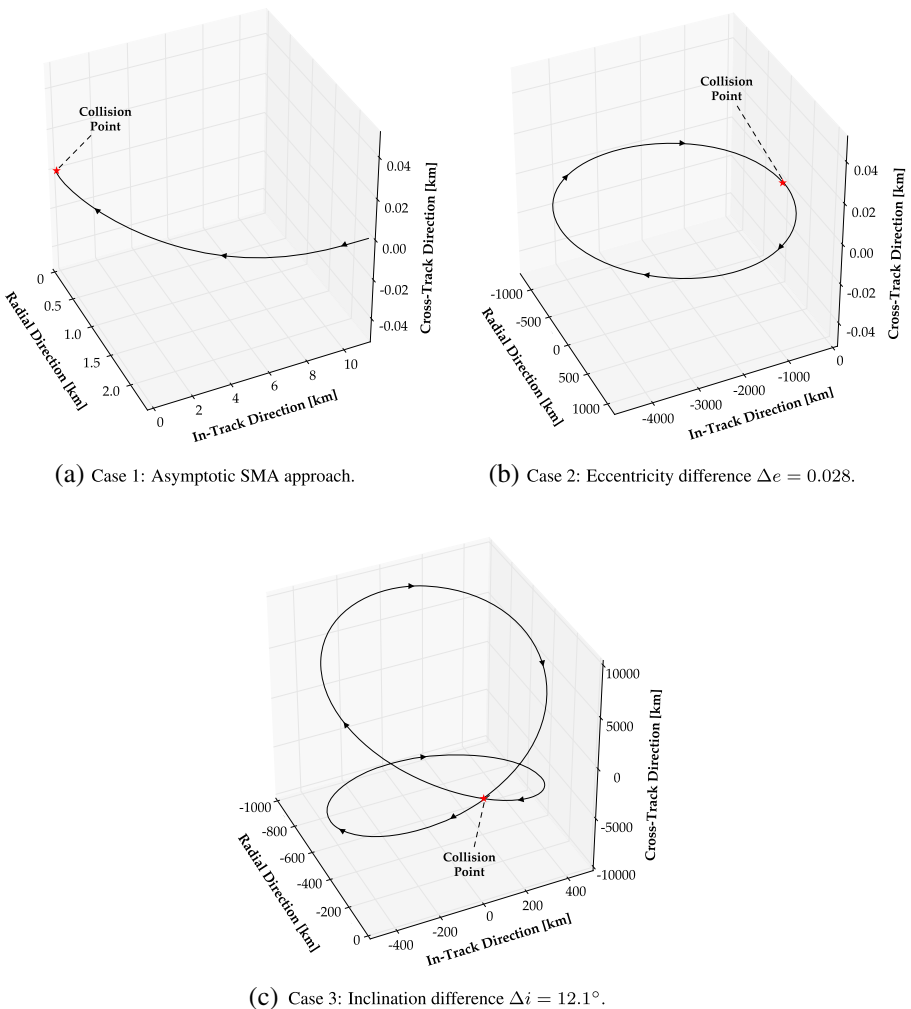


**Fig. 8** Relative Hill frame trajectories for representative GEO collision geometries

illustrates the resulting approach trajectories in the Hill frame for each of the three prototype scenarios in Fig. 6, using a 1 mN thrust level and specifying that the collision will occur 24 hours in the future, inasmuch as the bisection guidance method is not applied to alter the approach geometry.

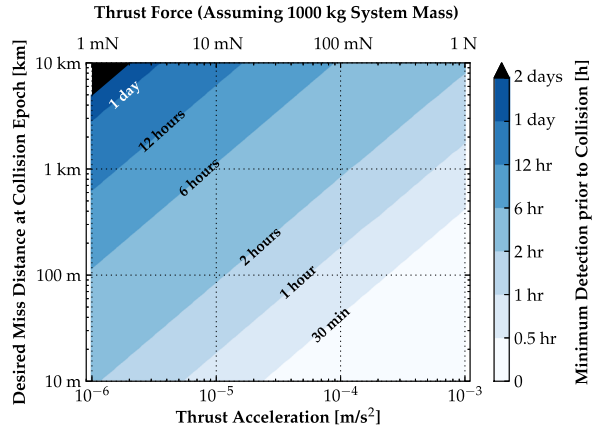
### Performance Bounds of Bisection Guidance Method

Performance bounds for the bisection guidance method are investigated with a two-dimensional sweep over thruster acceleration and miss distance at the collision epoch. For each thrust acceleration and desired miss distance, an auxiliary bisection technique is used to evaluate the minimum detection time required to maintain the surveyed miss distance at the collision time, i.e., the latest possible time that the debris object can be detected such that the re-orbit system can still evade the object while achieving the desired miss distance. As it is more advantageous for the re-orbit system the earlier it detects a conjuncting object—since resulting efficiency factors will be closer to the  $\gamma = 1$  maximum—this performance study illustrates worst-case, full-radial performance ( $\gamma = 0$ ) under best-case knowledge, that is, perfect chief and deputy initial conditions, no navigation or force model errors, etc.

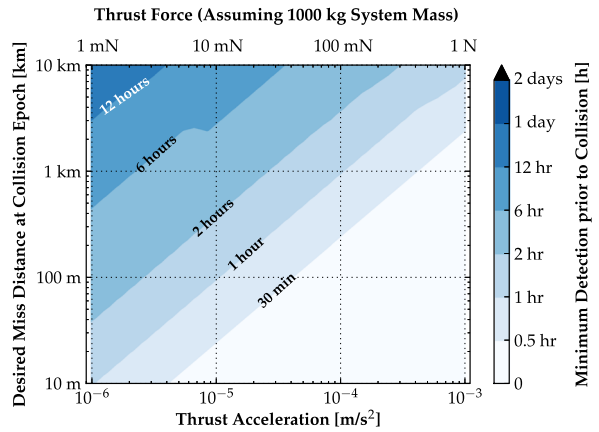
Figure 9 shows bisection performance bounds for each of the three representative collision scenarios in Fig. 8. Thrust accelerations ranging from  $10^{-6}$  m/s<sup>2</sup> to  $10^{-3}$  m/s<sup>2</sup> (i.e., 1 mN to 1 N of thrust force for a 1000 kg re-orbit system) are surveyed in tandem with miss distances ranging from 10 m to 10 km at the collision epoch. For example, if Case 1 approach geometry is assumed, Fig. 9a shows that a re-orbit system with  $10^{-6}$  m/s<sup>2</sup> of thrust acceleration requires 6 hours prior to the predicted collision epoch, at minimum, to miss this object by  $\sim 100$  m using the bisection guidance strategy. If the object is detected earlier than this bound, the resulting efficiency factor will improve; conversely, if the object is detected any later than this bound, bisection root-bracketing fails, and the specified miss distance is no longer achievable given the maneuverability of the re-orbit system. Note the latter does not state a collision *will* occur; rather, the desired miss distance is not achievable. In this situation, the assumption of continuous orbit raising enforced via the thrust vector constraint  $0^\circ \leq \alpha \leq 180^\circ$  could be relaxed to mitigate collision risk by temporarily allowing a negative SMA rate for this purpose.

The contours in Fig. 9 illustrate that as the thrust acceleration decreases, and the desired miss distance increases, the minimum required detection time rises exponentially. This is an intuitive result, for the less maneuverability a re-orbit system has, the sooner its guidance subsystem must know in advance of a predicted conjunction to begin altering the in-plane thrust angle such that the desired miss distance is achieved at the collision epoch. The white triangular regions in the southeast corners of Fig. 9 are those regions in this parameter space in which less than 30 minutes of lead time are required to miss the derelict using a full radial burn ( $\gamma = 0$ ). Interestingly, performance bounds improve as the relative velocity of the encounter increases, e.g., using  $10^{-6}$  m/s<sup>2</sup> of thrust acceleration and a 100 m miss distance, Case 1 in Fig. 9a requires a minimum detection time of approximately 6 hours, but this is reduced to approximately 3 hours in Fig. 9c for Case 3 geometry. This is a consequence of faster relative motion between the re-orbit system and conjuncting object at the collision

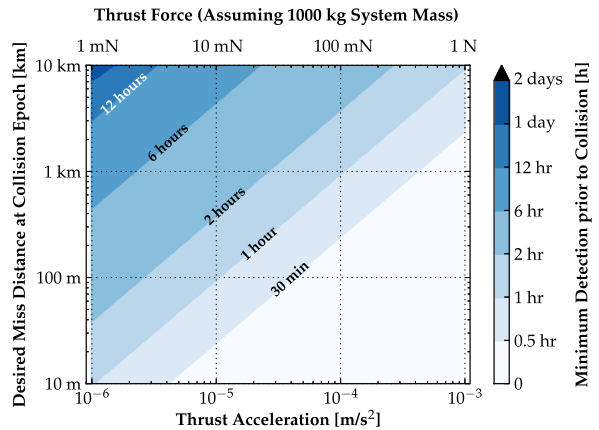
**Fig. 9** Performance bounds of bisection method for derelict avoidance, illustrated for various miss distances with the prototype GEO collision geometries in Figs. 6 and 8



(a) Case 1 performance: Asymptotic SMA approach.



(b) Case 2 performance: Eccentricity difference  $\Delta e = 0.028$ .



(c) Case 3 performance: Inclination difference  $\Delta i = 12.1^\circ$ .

epoch. Using a least-squares curve-fitting tool, the performance plots for Cases 1 and 3 in Fig. 9a and c can be approximated by the analytic functions

$$t_{\min}(\tilde{x}) \approx \exp(0.2396\tilde{x}^2 + 0.4124\tilde{x} + 0.2184) - 0.5572 \quad [\text{Case 1}] \quad (14)$$

$$t_{\min}(\tilde{x}) \approx \exp(0.2075\tilde{x}^2 + 0.4201\tilde{x} + 0.2583) - 0.9666 \quad [\text{Case 3}] \quad (15)$$

where  $\tilde{x} \equiv \frac{1}{\sqrt{2}} [\log_{10}(a_{\max}) - \log_{10}(d_{\text{miss}})]$ . In this formulation,  $a_{\max}$  is the thrust acceleration ( $\text{m/s}^2$ ),  $d_{\text{miss}}$  the desired miss distance (km), and  $t_{\min}$  the minimum detection time (hours) required to maintain  $d_{\text{miss}}$  at the collision time. The coefficient of determination that measures goodness of fit is  $\mathcal{R}^2 = 0.976$  for Case 1 and  $\mathcal{R}^2 = 0.980$  for Case 3, indicative of a good fit to the minimum detection times evaluated over the thrust/distance parameter space in Fig. 9.

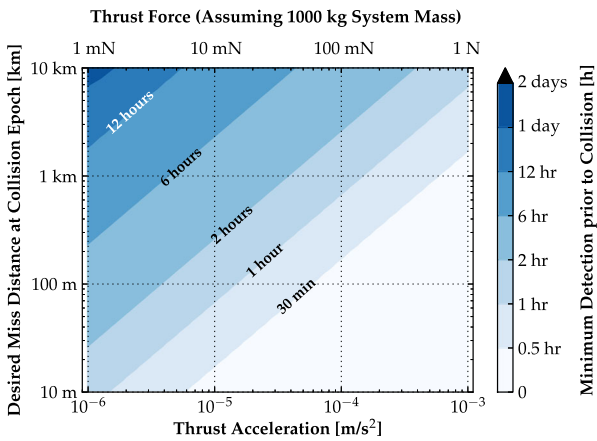
Note that although bisection performance bounds for Cases 2 and 3 in Fig. 9b and c are qualitatively similar, a bump observed on the 6-hour contour line in Fig. 9b is not exhibited in Fig. 9c. When computing minimum detection times in Fig. 9, trajectories are propagated using maximum available thrust in both the positive radial ( $\hat{o}_r$ ) and negative radial ( $-\hat{o}_r$ ) directions, since these directions both correspond to  $\gamma = 0$  (i.e.,  $\alpha = 0^\circ$  and  $\alpha = 180^\circ$ , respectively). As a consequence of the approach geometry for Case 2 in Fig. 8b, thrusting in the  $-\hat{o}_r$  direction gives larger miss distances southwest of the bump, and thrusting in the  $\hat{o}_r$  direction gives larger miss distances northeast of the bump. This observed “bump discontinuity” does not appear in Cases 1 and 3, since thrusting in the  $-\hat{o}_r$  direction provides larger miss distances across the entirety of the parameter space in these conjunction scenarios.

### Comparison with Coasting Guidance Method

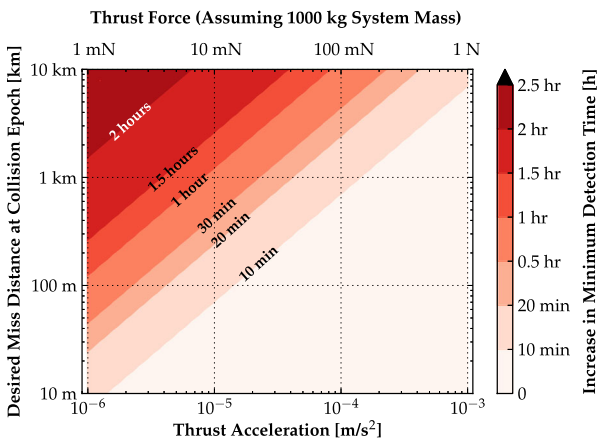
The bisection method developed in this paper applies maximum available thrust in the radial/in-track plane of the local orbit frame to evade a conjuncting debris object. Therefore, it is assumed that maximum available thrust is always applied to the re-orbit system during both orbit raising and collision avoidance. In the case of the former, the thrust vector is oriented in the in-track direction to maximize the rate of increase of SMA, and in the case of the latter, the bisection guidance method is used to alter the in-plane thrust angle such that the desired miss distance is achieved at the predicted collision epoch. In practice, executing the required thrust heading change could be challenging, especially for spacecraft with thrusters fixed in the body frame, which would have to execute an attitude maneuver to achieve the thrust vector heading  $\alpha$  commanded by bisection guidance. An alternate method for collision avoidance would be to simply turn-off the thrusters (i.e.,  $\mathbf{a}_t = \mathbf{0}$ ) and coast for a period of time, until the conjuncting object has been suitably avoided.

It is thus useful to compare the bisection performance bounds in Fig. 9 with the minimum detection times required to coast and still achieve the desired miss distance given the thrust acceleration of the re-orbit system. Recall that the worst-case efficiency factor of  $\gamma = 0$  is applied to quantify the minimum detection times illustrated for each of the three test cases in Fig. 9. The efficiency factor for bisection guidance improves the earlier the conjunction is detected, and Fig. 9 shows how late a conjuncting object can be detected such that the desired miss distance can still be achieved

with maximum available thrust fully oriented in the local radial direction. If it is more preferable to coast, Fig. 10 shows how late a conjuncting object can be detected such that the desired miss distance can still be achieved if the thrusters are turned-off until the predicted collision epoch. Case 3 coasting performance in Fig. 10a is qualitatively similar to bisection performance in Fig. 9c, but the difference in minimum detection times between the two guidance methods is illustrated in Fig. 10b. As shown in Fig. 10b, coasting always requires more lead time than bisection guidance requires – although a radial thrust heading or an absence of thrust can both guarantee a desired miss distance at the predicted collision epoch, the conjuncting object must be detected sooner if the re-orbit system is going to coast for collision avoidance rather than execute bisection guidance. This increase in the minimum detection time is amplified for smaller thrust levels and larger miss distances. Further, the SMA



(a) Case 3 performance: Inclination difference  $\Delta i = 12.1^\circ$ .



(b) Case 3 performance compared with performance in Figure 9(c).

**Fig. 10** Comparison of performance bounds for coasting method with those of bisection guidance method

has no secular increase during coasting periods, which is not preferable in the case of a low-thrust ADR system attempting to re-orbit derelict GEO objects as rapidly as possible.

## Conclusions

A continuous-thrust guidance strategy for debris avoidance during low-thrust re-orbit to a super-synchronous disposal orbit is investigated in this paper. The guidance law employs a bisection root-finding method to converge on the in-plane thrust angle that gives the desired miss distance at the predicted collision epoch, inasmuch as sufficient lead time is available prior to the conjunction. Designed with simple-yet-robust autonomy in mind, this bisection guidance strategy is ultimately a component of a larger, “sense and avoid” system to mitigate collision risk during orbit raising at end-of-life while minimizing human-in-the-loop requirements. When coupled with environmental sensing and an onboard, relative state estimator, bisection guidance can be applied to safely avoid specified “no-fly” regions around conjuncting derelicts, while continuing to increase the semimajor axis during a re-orbit. The performance bounds quantified in this paper illustrate that for typical conjunction velocities probable during GEO re-orbit, a desired miss distance of 1-2 km requires less than 12 hours of lead time for all surveyed thrust levels ranging from  $10^{-6}$  m/s<sup>2</sup> to  $10^{-3}$  m/s<sup>2</sup>. To compliment Reference [10]—which shows that conjunction challenges during GEO re-orbit can be reduced by increasing the thrust level and/or timing the start of the re-orbit burn appropriately—this paper demonstrates that any remaining collision risk can be safely mitigated with bisection guidance for online avoidance of debris objects.

**Acknowledgments** The authors would like to acknowledge the U.S. Department of Defense and the National Defense Science and Engineering Graduate Fellowship (NDSEG), the program through which funding for this research was obtained. The authors would also like to thank the anonymous reviewers who strengthened the content of this manuscript.

## References

1. Johnson, N.: Protecting the GEO environment: Policies and practices. *Space Policy* **15**, 127–135 (1999)
2. Jehn, R., Agapov, V., Hernandez, C.: The situation in the geostationary ring. *Adv. Space Res.* **35**, 1318–1327 (2005)
3. Chrystal, P., McKnight, D., Meredith, P.: *Space Debris: On Collision Course for Insurers?* Tech. rep., Swiss Reinsurance Company Ltd (2011)
4. Anderson, P.V., Schaub, H.: Local debris congestion in the geosynchronous environment with population augmentation. *Acta Astronaut.* **94**, 619–628 (2014)
5. Flohrer, T.: Classification of Geosynchronous Objects: Issue 16, Tech. Rep. 1, European Space Operations Centre (2014)
6. Jehn, R., Hernandez, C.: International practices to protect the geostationary ring. *Space Debris* **1**, 221–233 (2001)
7. NASA: Process for Limiting Orbital Debris, NASA-STD-8719.14 Change 4, National Aeronautics and Space Administration (2009)

8. Schaub, H., Moorer, D.F.: Geosynchronous large debris reorbiter: Challenges and prospects. *J. Astronaut. Sci.* **59**(1-2), 165–180 (2012)
9. Bombardelli, C., Pelaez, J.: Ion beam shepherd for contactless space debris removal. *J. Guid. Control. Dyn.* **34**(3), 916–920 (2011)
10. Anderson, P.V., Schaub, H.: Conjunction challenges of low-thrust geosynchronous debris removal maneuvers. *Acta Astronaut.* **123**, 154–164 (2016)
11. Schaub, H., Junkins, J.L.: Dynamics and control of micro-robot swarms: Planar Motion and State Estimation, Tech. rep., Texas A & M University (1998)
12. Leonard, N.E., Fiorelli, E.: Virtual leaders, artificial potentials and coordinated control of groups. In: Proceedings of the 40th IEEE Conference on Decision and Control (2001)
13. Junge, O., Ober-Blobaum, S.: Optimal Reconfiguration of formation flying satellites. In: Proceedings of the 44th IEEE Conference on Decision and Control (2005)
14. Izzo, D., Pettazzi, L.: Autonomous and distributed motion planning for satellite swarm. *J. Guid. Control. Dyn.* **30** (2007)
15. Bennet, D.J., McInnes, C.R.: Pattern transition in spacecraft formation flying via the artificial potential field method and bifurcation theory. In: Proceedings of the 3rd International Symposium on Formation Flying (2008)
16. Tatsch, A.R.: Artificial Potential Function Guidance for Autonomous In-Space Operations. PhD thesis, University of Florida (2006)
17. Louembet, C., Deaconu, G.: Collision avoidance in low-thrust rendezvous guidance using flatness and positive B-Splines. In: Proceedings of the 2011 American Control Conference (2011)
18. Epenoy, R.: Fuel optimization for continuous-thrust orbital rendezvous with collision avoidance constraint. *J. Guid. Control. Dyn.* **34** (2011)
19. Richards, A., Schouwenaars, T., How, J.P., Feron, E.: Spacecraft trajectory planning with avoidance constraints using mixed-integer linear programming. *J. Guid. Control. Dyn.* **25** (2002)
20. Mao, Z.-H., Feron, E., Bilimoria, K.: Stability of intersecting aircraft flows under decentralized conflict avoidance rules. In: Proceedings of the AIAA Guidance, Navigation, and Control Conference, AIAA, pp. 1042–1052 (2000)
21. Schaub, H., Junkins, J.L.: Analytical Mechanics of Space Systems, 2nd edn. American Institute of Aeronautics and Astronautics, Inc. (2009)
22. Prussing, J.E., Conway, B.A.: Orbital Mechanics, 2nd edn. Oxford University Press (2013)